Research Article

Effectiveness of Zinc Concentration on the Structural and Electrical Properties of Cu₂ZnSnS₄ nano-powder Prepared by Sol-gel Method

A.H. Salama[1], A. M. Youssef [2] and F. F. Hammad [2]

[1.] *Physical Chemistry Department, National Research Centre, El-Buhouth St., Dokki, Cairo 12622, Egypt*
[2.] *Inorganic Chemistry Department, National Research Centre, El-Buhouth St., Dokki, Cairo 12622, Egypt*

ARTICLE INFO

ABSTRACT

The current study uses a sol-gel method to concentrate Zn, particularly 0.1, 0.3, and 0.5 mole, with the use of nitrate and chlorides for synthesizing Cu_2ZnSnS_4. The XRD diffraction pattern suggests the obtained powders with kesterite structures peaked at (112), (220), and (312) phases that correspond to CZTS kesterite structure. Studying the impact of temperature and frequency on the electrical conductivity of the Dc and Ac- electric fields helped us carry out electrical studies. Frequency range from 50 Hz to 5 MHz and temperature range from room temperature to 150 0C. Based on this study, the hopping conduction mechanism is the most suitable mechanism for conduction in the samples. Using similar frequency and temperature ranges, we succeeded in evaluating how to use a variety of Zn concentrations to determine the dielectric constant of some doped samples and un-doped CTS. The dependence of ε' on concentration was found in this study.

Introduction

Thin film solar cells have recently used kesterite structured Cu_2ZnSnS_4 (CZTS) to function as a layer for adsorption, to replace GdTe and Cu $(In,Ga)Se_2$(CIGS), as it has no elements which are toxic and rare [1-3]. Since there is a need to reduce the cost of PV industry producing > 150 GWP / year of thin film panels, scientists pay attention to kesterite compounds to feature earth-abundant photovoltaic (PV) absorber layers. What is more, the kesterite compound can be an effective photovoltaic material since it entails optoelectronic properties, e.g., a tunable band gap (1.0 – 1.5 eV) as well as a high absorption coefficient ($\sim 10^4 – 10^5$ cm^{-1}) [4 - 8]. Some studies reported that CZTS composites preparation technique determines solar cell power conversion efficiency (PCE) [9]. Synthesizing CZTS can be carried out with a variety of methods, including sol-gel method [10], RF sputtering [11], thermal evaporation [12], screen printing [13], electro-deposition process [14], spin coating [15], spray pyrolysis [16], SILAR method [17], electron beam evaporation [4], and pulsed laser deposition [18]. As reported in a recent study by Subramanian et al., the chemical bath deposition method may contribute to depositing CZTS film with PCE of 1.34% [19]. Besides, Sudip K. Saha et al. found that a PCE of 0.9% results when using hot injection to prepare CZTS- Fullerene hybrid p – n junction solar cells [20], whereas Suryawansi et al., reported the highest value of PCE of about 3.81% when using SILAR method to prepare CZTS [21]. The electrical conductivity for the kesterite-like compounds was not reported in any previous research. We accordingly reported the application of a sol-gel method to concentrate Zn, particularly 0.1, 0.3, and 0.5 mole %, with the use of a couple of sols as precursors which are nitrates and chlorides, for synthesizing a quaternary compound semiconductor Cu_2ZnSnS_4. A variety of tools, such as SEM + EDAX, XRD, and IR, structurally characterize the synthesized compounds. Estimating the conduction mechanism was done during our study of the alternating current electrical conductivity functioning temperature and frequency. We eventually used similar frequency and temperature ranges for studying the dielectric properties. Developing less costly CZTS solar cells could be the contribution of this study.

---

2. Experimental:

Being the most popular method used for the preparation of metal oxide nanocomposites, the citrate technique base on pechini method [22] was used to prepare Nano-sized powders of un-doped and co-doped Kesterite structure with Zn as a dopant. For doping metal, we used three Zn ions concentrations, namely 0.1, 0.3 and 0.5 mol. %, to prepare four samples as well as doped and undoped samples. In this method, we used ethylene glycol and citric acid to function as gel former and complex in agent. $C_2H_4(OH)_2$ (99%, Chem. Pure), Indium chloride (99%, Aldrich), $SnCl_4.5H_2O$ (99%, Aldrich), and $C_6H_8O_7$ (99.5%, Pharmaceutical Chemicals) were the starting materials. For chelating metal cations at the CA: Mex+ mol at ratio of 2:1, we added citric acid (CA). After the interaction took place for 15 minutes, we added ethylene glycol (EG) to solution at a CA: EG molar ratio of 80:20. For promoting the polymerization and esterification reactions 150 °C was used to obtain, heat, wash, and stir the colorless solutions. After we eliminated water and nitrous oxides, we obtained a clear resin. For removing organic substances, we charred the polymeric resin.

For obtaining the nano-sized ceramic powder, we produced, and ball milled the brown powder for 18 hours at 500 °C. For adjusting the stoichiometry, we used some previously prepared samples to carry out chemical analysis.

We used X-ray diffractograms, provided with a computer-controlled X- ray diffractometer "The PHILIPS® MPD X'PERT diffractometer formally made″, to identify the whole prepared powder sample's crystalline structure. A Copper-tube operating at 40 Kv and 30 mA constituted the X-ray tube we used. We used Rietveld software MAUD 2.074 [23] to calculate the micro-strain, the average crystallite size, and X- ray diffractometer with a CuK_α radiation (λ= 1.5418 ˚A) the lattice parameter.

For measuring the electrical conductivity and dielectric properties, for the entire investigated samples in the temperature range from 25 to 150 o C and frequency range from 42 Hz to 5 MHz, we used the computerized LCR Bridge (HIOkI model 3532-50 LCR Hi Tester). To establish conductivity equilibrium values, we performed the measurements after adequate time at each temperature.

To conduct our experiment, we obtained the real as well as imaginary parts of the complex dielectric permittivity ε^* ($\varepsilon^*=\varepsilon-j\varepsilon'$), assuming that a circuit made up of an ideal capacitance in parallel with a pure (ohmic) resistance Rp equals the cell we studied.

At all temperatures and frequencies considered, the measured capacitance is used for calculating the real part of dielectric function (constant) ε' of doped and un -doped CTS nano powders using the following eqn.

$$\varepsilon' = (C_p d/ \varepsilon_o A)$$

where: ε_o is the permittivity of free space equal to 8.85 x 10^{-12} F/m. C is the capacitance, d is the thickness, A is the area of the measured disc sample.

The observed values of the resistance for the samples tested contributed to the calculation of the frequency and temperature dependence of ac-conductivity σ_{ac}. The relation ($\sigma_{ac} = A\omega^s$) was used to calculate the ac-conductivity, with $0 \leq S \leq 1$, ω being the angular frequency of the applied ac field and A = π N2e2/6KBT (2α) is a constant, e is the electron charge, T is the temperature, α is the polarizability of a pair of sites, and N is the number of sites per unit volume among which hopping takes place.

3-Results and discussion:

3.1: X-ray diffraction studies

Figure (1) shows X-ray diffraction pattern of undoped CTS and doped CTS with zinc concentrations of 0.1, 0.3 and 0.5 mole %, indicating a couple of things: the diffraction angle 2θ varied from 20 to 800, and the whole samples were crystallized efficiently. Tetragonal kesterite type structures with peaks attributed to the (112), (220) and (312) phases corresponding to the kesterite structure of the CZTS (JCPDS 01 – 75-4122) [24 -26] constituted the samples' XRD pattern. Figure (2) indicates alternating cation layers of CuSn, CuZn, CuSn and CuZn at z= 0, 1/4, 1/2 and 3/4 in the direction of the crystallographic c-axis, characterizing the kesterite type structure.

As table 1 shows, there was a dramatic variation among the samples of the full width at half-maxima (FWHM) corresponding to (1 1 2) peak, as found from the XRD spectra. In addition, binary or ternary phases had no XRD patterns. As we observed, the XRD patterns of powder samples prepared showed zero preferential growth. The Scherrer equation (d = k λ / β Cos θ), where k is a constant of 0.9 and β is the full width at half maximum (FWHM) of the most intensive peak for (112) plane, was used to estimate the annealed CZTS average crystalline size of 44, 41, 39 and 38 nm, were the powderaverage crystal size estimated.

3.2 Microstructure:

Powder composition obtained from EDAX spectroscopy of 0.3 mole % of Zn ions coupled with SEM images of undoped CTS shown in Figure (3).
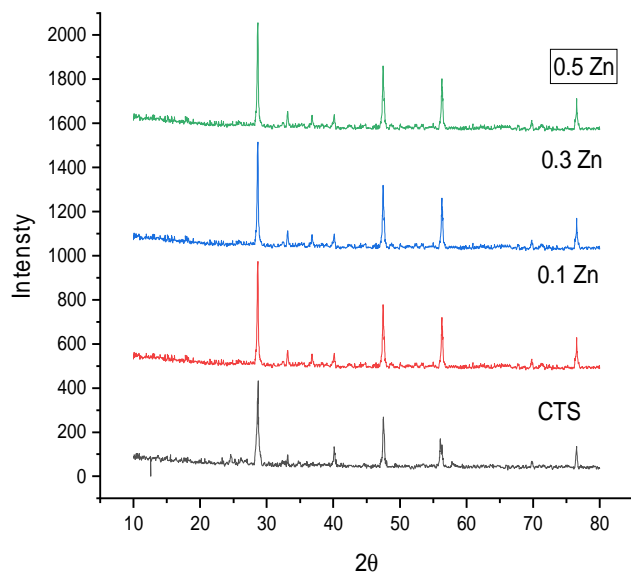
.

Fig. 1. X-ray diffraction pattern for un-doped CTS and doped samples with different conc. of Zn^{+2} ions.
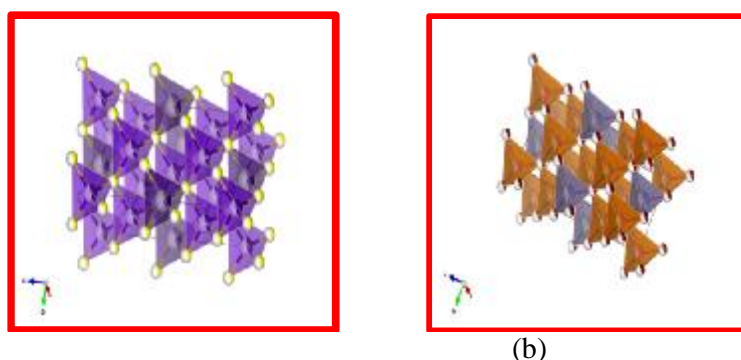

|(a)|(b)|

Fig. 2. The cation distribution of Cu, Zn and Sn of undoped CTS and doped with 0.3 mole % of Zn Kesterite – type structure.

Table 1. Calculated lattice parameters from the XRD- pattern corresponding to the dominant (1 1 2) peak of CZTS.

Sample	Crystallite size (nm)	2θ(º)	d-spacing (Å)	Lattice parameter		Direct cell volume (Å^3)
				a(Å)	c (Å)	
CTS	44	28.52	3.127	5.407	10.832	316.702
CZTS-0.1	41	28.43	3.136	5.438	10.838	320.486
CZTS-0.3	39	28.18	3.164	5.453	10.85	322.638
CZTS-0.5	38	28.37	3.143	5.434	10.84	320.107

3.2: Microstructure:

Powder composition obtained from EDAX spectroscopy of 0.3 mole % of Zn ions coupled with SEM images of undoped CTS shown in figure (3). For proving a successful process for the fabrication of kesterite-like structures, it is vital to study CTS surface morphology. A series

of closed-packed CTS and CZTS grains without void spaces or porous structure is shown in Figures 3 (a) and (b). When we compared that with the average crystal size (nm) estimated, we found that a polycrystalline structure features the CZTS and CTS powder, as shown in table (1). Table (2) as well as figures 3 (c) and (d) show a

graphical representation of the elemental composition estimated from EDAX.
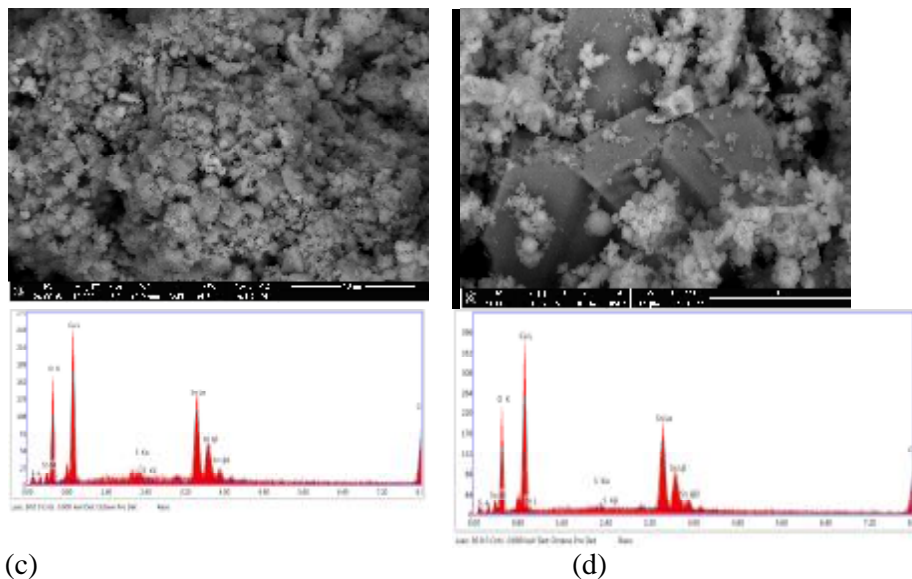
(c)   (d)

Figure (3): SEM micrographs for undoped sample (a) and doped with 0.3 mole % of Zn ions **(b),** (c) and (d) represents EDAX analysis of the same two samples

Table 2. the elemental composition from EDAX analysis for undoped CTS and doped with 3 mole % of Zn ions.

elements	CTS	CZTS
	Atomic %	Atomic %
O	48.25	51.07
S	2,44	0.8
Sn	10.11	11.26
Cu	39.2	36
Zn	…….	0.86

A S- poor composition in CZTS sample (S/Metal < 11), as exhibited by the EDAX analysis, suggesting how S and the other metal into the precursors interacted sufficiently.

3.3. Infrared spectroscopy:

FTIR was carried out for the purpose of complementary characterizations. Figure (4) shows how FTIR responded to the 4 samples under test, showing how a variety of bands at 630, 1129, 1651, 2369 and 3460 cm^{-1} are existing. Besides the typical signature of thiourea (3460 cm^{-1}) and water [27], we found that metal – thiourea complexes affected the observation of peaks [28]. Banding frequency as well as oxygen stretching cause the emergence of bands around 900 -1600 cm^{-1}. The resonance interaction between vibration modes of sulfide ions in the crystal cause the existence of weak additional bands at 950 and 884 cm^{-1} [29]. ZnS band (i.e corresponding to sulfides) assigns the peak at 630 cm^{-1}. The S-H thiol functional class causes the characteristic absorptions at 2938 and 2369 cm^{-1} [30].

3.4: Dielectric studies for the prepared samples as a function of frequency and temperature:

According to Shukla et al., (2016) [31] and many other studies, subscribing to many polarization types (orientation, space charge iconic, and electronic polarization) reasons why ε' decreases when we increase the frequency of a polar material. The changes in valence states of space charge polarization and cations cause this polarization to occur. The lag of electric dipoles that happens after the fast variation of the alternating electric field implemented makes the dielectric constant not affected by frequency in the case of higher frequencies.

The displacement of the valence electrons relative to the positive nucleus leads to the existence of electronic polarization in case we have a high frequency up to 10^{16} Hz. On the other hand, the shift of positive and negative ions causes the iconic polarization at 10^3 Hz. Regarding dipole polarization, it takes place in a material that entails molecules with permanent electric dipole moments, at approximately
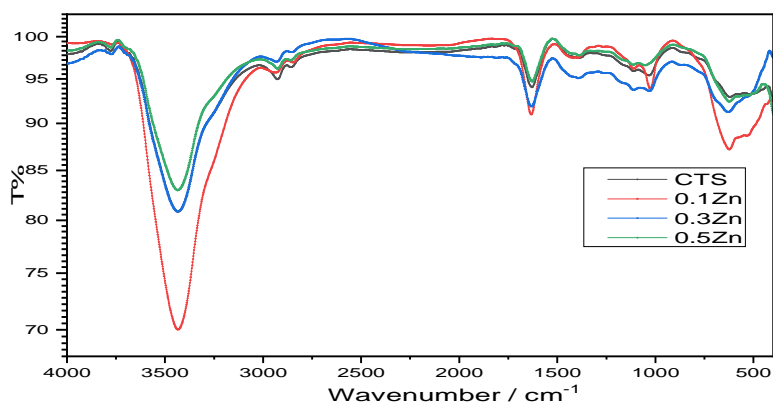
Fig. 4. FTIR spectra of un-doped CST and doped with different conc. of Zn ions.

10^{10} HZ. As for the final polarization type, the space charge polarization, impedance mobile charge carriers by interfaces cause it to emerge, at from 0 to 10^3 Hz frequency ranges. As proved by Hegab and El-Mallah (2009) [32], the dielectric material total polarization is the source of the sum of the 4 aforementioned polarization types. According to the findings of the running study and as represented in figure (5), we can infer that each dopant's magnetic or electric effect as well as the interfacial effects of doped metal oxide nano-powders and the CTS crystal structure probably cause dielectric constant ε' to function at high values.

Since we performed the study at different frequency ranges varied from 42 Hz to 5 MHz, Fig. 5 provides a graphical representation of the dielectric constant of un-doped CTS ceramics and doped samples with 0.1, 0.3 and 0.5 mole % of Zn ions we observed at temperature range from room temperature to 150°C. Generally speaking, when we increase the value of the entire ceramic sample's frequency, the values of dielectric constant ε' decrease. On the other hand, when we increase the entire ceramic sample temperature, the values dielectric constant ε' increase. When we have a maximum value at low frequencies, the values of dielectric constant ε' decrease dramatically and collapse to the extent that it depends less on frequency. We can eventually attain a constant value of dielectric constant ε' when it undergoes microwave frequency.
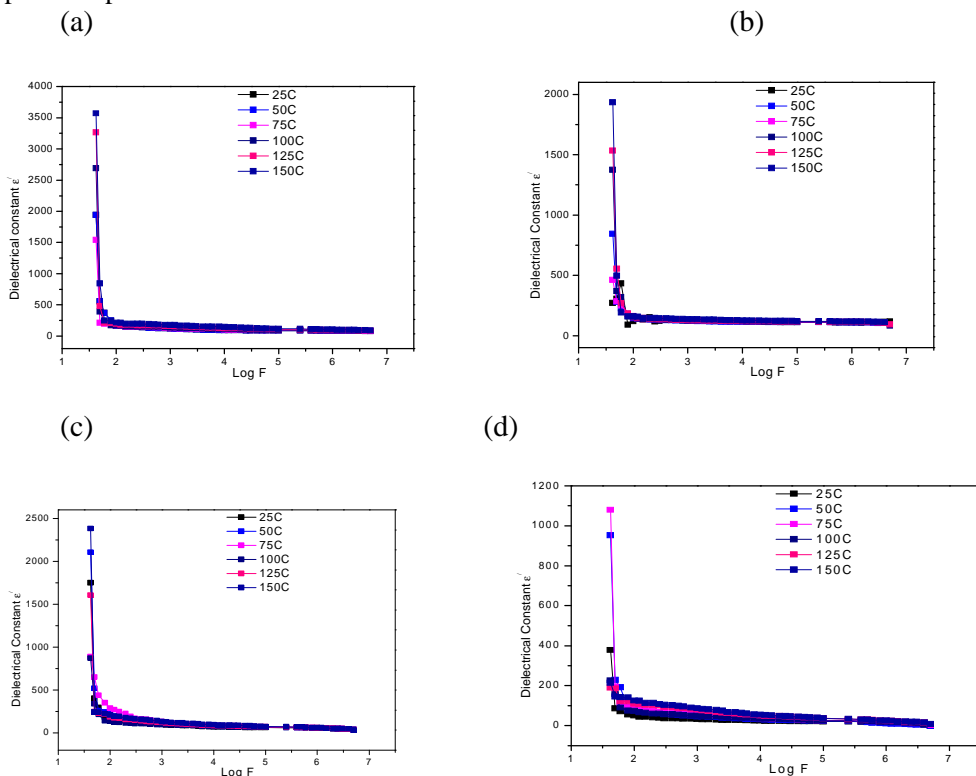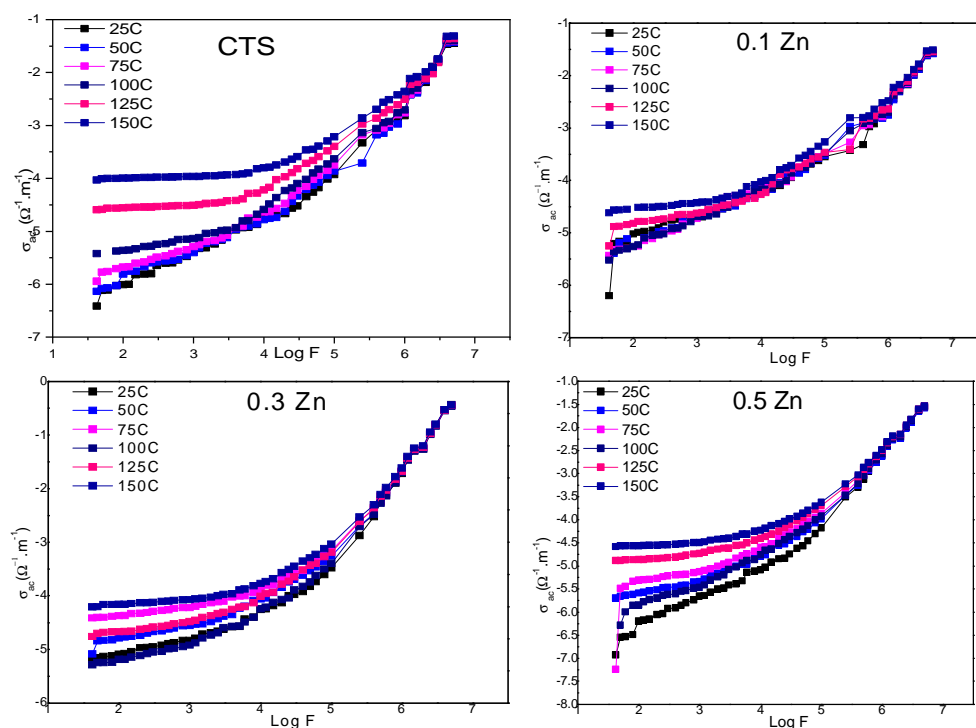
(a)

(b)

(c)

(d)

Fig. 5. The variation of dielectric constant with frequency at different temperatures for (a) un-doped CTS, (b) 0.1mole % CZTS, (c) 0.3 mole % CZTS and (d) 0.5 mole % CZTS

We can conclude that determining the dielectric constant ε′ value relies upon the way Zn ions are concentrated. Within Zn ions concentration, the un-doped sample varied from 2.045×10^3 to 3.79×10^3 reaching the maximum value at 42 Hz frequency and with increasing temperature from room temperature to $150\ {}^0$C. When a sample of 0.1 mole % exists, the dielectric constant ε′ value varies from 2.06×10^2 to 2.017×10^3 at the same frequency and temperature range, while its value ranges from 1.838×10^3 to 2.5×10^3 for 0.3 mole % sample. Eventually, the dielectric constant ε′ value ranges between 3.97×10^2 and 2.26×10^2 for 0.5 % sample. Room temperature to 150^0C at 42 Hz causes such diverse values. So, we can conclude that the presence of Zn ion in the crystal lattice decreases the dielectric constant of the prepared samples which may be because Zn ion acts as a trap of electrons at the interface boundary, and as a result polarization decreases and dielectric constant values as well.

3.5. Frequency and composition dependence of AC electrical conductivity

We study the ac conductivity for undoped CTS and doped CTS which entail 0.1, 0.3, and 0.5 mole % of nano- ZnO. The hopping conduction is typically used to specify σ1 (ω). In terms of frequency (ω), a power law behavior characterizes ac conductivity.

Figure 6 shows how the frequency (50 Hz –5 MHz) causes the microwave conductivity of the samples under test to change. The whole samples witnessed an increase of conductivity every time we increase temperature, relying upon how the doped metal oxide is concentrated.

Fig 6. the variation of ac- electrical conductivity with frequency at different temperatures for (a) un-doped CTS, (b) 0.1mole % CZTS, (c) 0.3 mole % CZTS and (d) 0.5 mole % CZTS

To illustrate how the electrical behavior of material determines the frequency, we strongly recommend using the method of ac–conductivity measurement. Figure 6 shows how a variety of temperatures cause ac- conductivity (σac) to vary. As cited in Abdel-Karim et al., (2018) [33], Jonscher attempted to clarify this behavior, with the use of the following universal power law:

$$\sigma_{ac} = \sigma_{dc} + \sigma_1\ (\omega)$$
$$\sigma_{ac} = \sigma_{dc} + A\omega^s$$

Based on the above equations, assigning the frequency of σ_{dc} does not depend on frequency, as σ_{dc} is connected to dc- conductivity. The hopping conduction specifies σ_1 (ω) in a typical manner. In terms of frequency (ω), a power law behavior characterizes ac conductivity. Temperature determines A, the pre-exponential factor. A value between 0 and 1 features S, the exponent. The hopping conduction predominates if S has a value less than unity, while tunneling of localized motion characterizes the conduction if S enjoys a value more than unity. Two

carrier conduction mechanisms can depict the term $A\omega^s$, as follows:

● Quantum mechanical tunneling (QMT) via the barrier that separates the localized sites.

● Correlated barrier hopping (CBH) located above the same barrier.

As shown in Figure 6, the studied ceramic samples involve two frequency-dependent regions: the low-frequency region and the high-frequency region. The former is dispersed, while the latter does not depend on temperature. When the grain resistance is controlled by the grain boundary resistance, we can spot how the slope of ac-conductivity changes at the temperature. The conductivity increases when we increase the charged species so that entails enough energy to overcome the barrier at grain boundaries. The relation $(\sigma(\omega) = K\omega p [1 + (\omega/\omega p)]^n)$ describes the hopping frequency resulting from transition frequency.

Figure 7 shows the power law exponents (s) as a function of temperature for the studied four samples. As we see at both low- and high-frequency ranges, the s exponent decreases when we increase the temperature for undoped sample CTS, and its value is not higher than unity, so the observed behavior of s is appropriate with the correlated barrier hopping model (CBH) As assumed by Ben Taher et al. (2015) [34], such behavior has been stated by other research [35-39]. According to this model, the conduction occurs by bipolaron hopping process where two polarons hop over the potential barrier between two charged defect states $M^{2+} \leftrightarrow M^{3+}$ ions simultaneously and barrier height is correlated to the inter–site separation by a Columbus interaction. On the other hand, we found that at the low-frequency range, the s values for doped samples fluctuate with temperature and their values are lower than unity which ensures that the conduction here is CBH.

Otherwise, at higher frequencies, the grain boundaries are more effective and s values are more than unity so, we can declare that the conduction mechanism in this range is quantum mechanical tunneling (QMT) via the barrier.
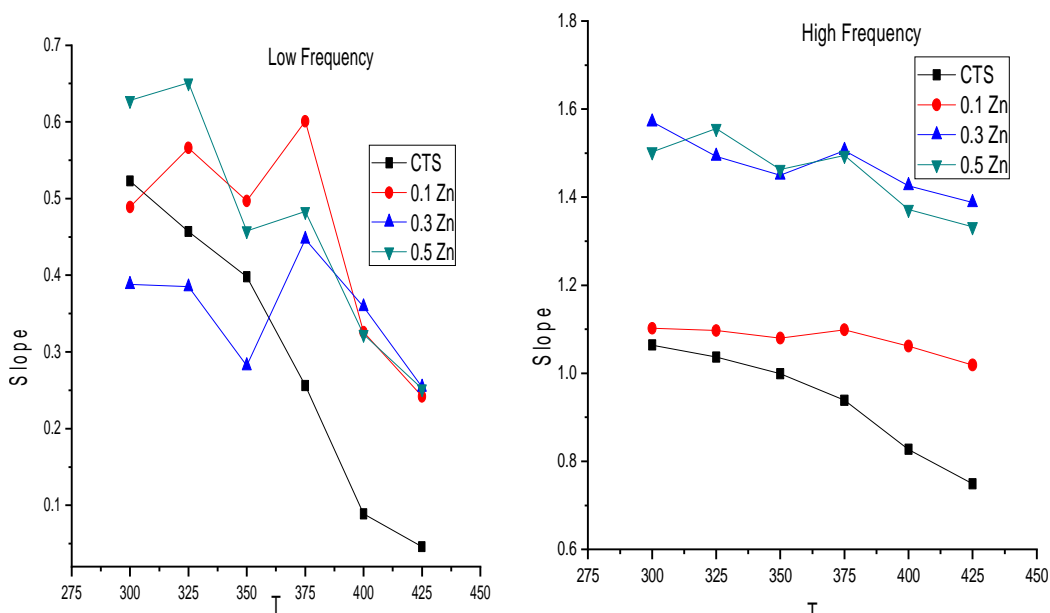

Fig. 7. the behavior of s with temperature for the studied prepared ceramic samples at low and high-frequency ranges.

4. Conclusion

Under a Kesterite-like structure, CTS and doped Kesterite structure with 3 different concentrations of Zn ions are successfully prepared by a sol-gel technique using mixed precursors of nitrates and chlorides. The prepared samples are structurally characterized by EDAX + SEM images which ensure that the prepared samples are polycrystalline closed-packed structures without void spaces or porous structures. XRD diffraction studies ensure the high crystalline feature of the prepared Kesterite ceramics in addition to the peak that appeared at (112), (220) and (312) phases declare the tetragonal Kessrite-like structure according to (JCPDS 01 – 75 – 4122). Through study FTIR – spectroscopy, we can declare the presence of Kesterite structure due to the presence of bands at 630, 1129, 1651, 2369, and 3460 cm^{-1} in addition to the typical signature of thiourea (3460 cm^{-1}) and water.

Through the study of the dielectric behavior of the prepared four samples we have a conclusion that the presence of Zn ion in the crystal lattice decreases the

dielectric constant of the prepared samples which may be due to the fact that Zn ion act as a trap of electrons at the interface boundary and as a result polarization decrease and dielectric constant values as well. The hopping conduction mechanism is the conduction

mechanism for our studied samples at low frequency whereas at high frequency range the quantum mechanical tunneling (QMT) is the preferred conduction mechanism.

References:
[1] A. Walsh; S.Y. Chen; S. H. Wei; X. G. Gong, Adv. Energy Mater. **2,** 400 (2012).
[2] T. Todorov; O. Gunawan; S. J. Chery; T. G. Monsabert; A. Prabhakar; D. B. Mitz, Thin Solid Films **519**, 7378 (2011).
[3] L. Choubrac; A. Lafond; C. Guillot-Deudon; Y. Moëlo; S. Jobic, Inorganic Chem. **51,** 3346 (2012).
[4] H. Katagiri; N. Sasaguchi; S. Hando; S. Hoshino; J. Ohashi and T. Yokota, Sol. Energ. Mat. Sol. C., **49**, 407 (1997).
[5] B. Shin; N. A. Bojarczuk; C. S. Jay and S. Guha, Appl. Phys. Lett. **101**, 053903 (2012).
[6] R. Haight; A. Barkhouse; O. Gunawan; B. Shin; M. Copel; M. Hopstaken and D. B. Mitiz, Appl. Phys. Lett., **98**, 253502 (2011).
[7] H. R. Jung; S. W. Shin; K. V. Gurav; M. G. Gang; J. Y. Lee; J. H. Moon and J. H. Kim, Electron. Mater. Lett., **12**, 139 (2016).
[8] J. Kim and B. Shin, Electron. Mater. Lett., **13(5)**, 373 (2017).
[9] J. Henry; K. Mohanray and G. Sivakumar, J. of Asian Ceramic Societies **4,** 81 (2016).
[10] K. Tanka; Y. Fukui; N. Moritake and H. Uchiki, Sol. Energy Mater. Sol. Cells, **95**, 838 (2011).
[11] J. S. Seol; S. Y. Lee; J. C. Lee; H.D. Nam and K. H. Kim, Solar Energy Mater. Solar cells, **75**, 155 (2003).
[12] R. Touati, M. B. Rabeh and M. Kanzari, Energy Procedia, **44**, 44 (2014).
[13] Z. H. Zhou; Y. Y. Wang; D. Xu and Y. F. Zhang, Sol. Energy Mater. Sol. Cells **94**, 2042 (2010).
[14] B. Ananthoju; A. Kushwaha; F. J. Sonia and M. Aslam, AIP Conf. Proc., **1512,**706 (2013).
[15] J. Wang; P. Zhang; X. Song and I. Gao, RSC Adv. **4**, 21318 (2014).
[16] N. E. Rodriguez; D. Sylla;Y. Sanchez; S. Lopez-Marino; X. Fontana; J. Lopez-Garcia; M. Placidi; A. Perez-Rodriguez; O. Vigil-Galan and E. Sauceda, J. Phys. D., Appl. Phys., **47**, 245101(2014).
[17] N. M. Shinde; D. P. Dubal; D.S. Dhawale; C. D. Lokhande; J. H. Moon, Mater. Res. Bull., **47**, 302 (2012).
[18] K. Moriya; K. Tanaka; H. Uchiki, JPN. J. Appl. Phys. **47**, 602 (2008).
[19] E. P. Subramanian; G. Rajesh; N. Muthukumarasamy; M. Thambidurai; V. Asokan and V. Velauthapillai, Indian J. of Pure Appl. Phys., **52**, 620 (2014).
[20] S. K. Saha; A. Guchhait and A. J. Pal, Phys. Chem. Chem. Phys., **14,** 8090 (2014).
[21] M. P. Suryawanshi; S. W. Shin; U. V. Ghorpade; K. V. Gurav; C. W. Hong; G. L. Agawane; S. A. Vanalakar; J. H. Moon; J. H. Yum; P. S. Patil; J. H. Kimand and A.V. Moholkar, Electro. Chim. Acta, **150,** 136 (2014).
[22] A. H. Salama ; A. M. Youssef ; H. A. Abbas ; F. F. Hammad, Interceram, **65 (4)**, 179 – 185 (2016).

[23] A. H. Salama, M, El-Hofy, Y. S. Rammah and M. Elkhatib, Advances in Natural science; Nanoscience and Nanotechnology, **6 (5),** 045013 (2015).
[24] Q. Guo; H. W. Hillhouse; R. Agrawal, J. Am. Chem. Soc., **131**, 11672- 11673 (2009).
[25] V. T. Tiong; Y. Zhang; J. M. Bell; H. Wang, Cryst. Eng. Comm., **16(20),** 4306 -4313 (2014).
[26] V, T. Tiong; J. Bell and H. Wang, Belilstein J. of Nanotechnolgy, **5**, 438 -446 (2014).
[27] S. Gorai; D. Ganguli and S. Chaudhuri, Cryst. Growth Des. **5**, 3875 (2005).
[28] K. Das; S. K. Panada; S. Gorai; P. Mishra and S. Chaudhuri, Mater. Res. Bull. **43**, 2742 (2008).
[29] K. Sooklal; B. S. Cullum; S. M. Angel and C. J. Murphy, J. Phys. Chem., **100,** 4551 (1996).
[30] M. Patel; I. Mulkhopadhyay and A. Ray, J. Phys. D.: Appl. Phys. **45**, 445103 (2012).
[31] N. Shukia; V. Kumar and K. Dwivedi, J. of Non-Oxide Glasses, **8(2)**, 47- 57 (2016).
[32] N. Hegab and E. El-Mallah, Acta Physica Polonica A **116 (6),** 1048- 1052 (2009).
[33] A. M. Abdel-Karim; A. H. Salama and M. L. Hassan, J. of Physical Organic Chemistry, e3851 (2018).
[34] Y. B. Tahr; A. Questati; N. K. Maaloul; K. Khirouni and M. Gargour, Applied Physics A, **120,** 1537 -1543 (2015).
[35] M. L. Hassan; A. F. Ali; A. H. Salama and A. M. Abd-Karim, J. of Physical organic Chemistry, **32(2),** 1-13 (2019).
[36] A. M. Farid; H. E. Atyia and N. A. Hegab, Vacuum **80 (4),** 284- 294 (2005).
[37] M. Ganaie and M. Zulfequar, Acta Physica Polonica A **128 (1),** 59 – 63 (2015).
[38] N. A. Hegab; M. Fadel; I. S. Yahia; A. M. Salem and A. S. Farid, J. of Electronic Materials **42 (12),** 3397 – 3407 (2013).
[39] A. Sharma; A. Kumar and N. Mehta, Measurement **75**, 69- 75 (2015).

Authors Contributions:
AH developed the process for the fabrication of Kesterite structure and performed electrical characterization, data analysis and contributed to the manuscript. AM analyzed the temperature dependent measurements. FF and AM performed structural characterization of Kesterite samples and contributed to the manuscript.

Declaration:
The authors declare that they have no known competing financial interests or personal relationships that could have appeared to influence the work reported in this paper.

Conflict of interest:
On behalf of all authors, the corresponding author states that there is no conflict of interest.

Data Availability:

The datasets generated during and/or analyzed during the current study are available from the corresponding author on reasonable request.